Intelligent Electrical Protection in Traditional Networks and Smart Grids

Intelligent Electrical Protection in Traditional Networks and Smart Grids

By

Salman Rezaei

Cambridge
Scholars
Publishing

Intelligent Electrical Protection in Traditional Networks and Smart Grids

By Salman Rezaei

This book first published 2024

Cambridge Scholars Publishing

Lady Stephenson Library, Newcastle upon Tyne, NE6 2PA, UK

British Library Cataloguing in Publication Data
A catalogue record for this book is available from the British Library

ISBN: 978-1-0364-1523-5
ISBN (Ebook): 978-1-0364-1524-2

TABLE OF CONTENTS

PREFACE

The term "protection" in electrical engineering refers to a set of devices and a logical strategy to decrease damage to electrical equipment and increase the availability of electrical energy. Primary protective gears like fuses and bimetals are preliminary devices that have been used in electrical circuits. With the growing electrical networks and increasing power and voltage in electrical equipment, the necessity of using secondary protection in electrical circuits has become prominent. The application of instrument transformers illuminates a way to implement secondary protection. Electromechanical protective devices provide insufficient reliability in terms of measuring quantities and operation speed.

With advancements in technology and emerging electronic, digital, and microprocessor-based elements, protective relays represent a significant increase in the reliability of electrical energy. Along with a significant improvement in generation and transmission devices, the complication of the electrical network and emerging transient and steady-state phenomena in the network and equipment, state-of-the-art protective devices have to be represented to improve the certainty of electrical protection. The design of algorithms for the analysis and processing of electrical signals and the designation of additional binary and analog measurements to the relays have caused practical enhancements, which comply with the complexity of the electrical grid. Nevertheless, the emergence of a variety of nonlinear electrical phenomena due to the complexity of the extensive networks composed of different kinds of power electronic devices and active and passive elements with different specifications potentially causes maloperation of protective relays. In addition to that, the high penetration of renewable energy resources into the utility system urges more series implementation of protection requirements to maintain the system in a safe condition.

Besides the widespread traditional network, the new approach in the electrical grid known as the "smart grid" represents a bidirectional communication between generation and consumption to deliver electrical energy more efficiently. Renewable energy resources have a significant role in supplying consumers in the smart grid. As the smart grid requires a self-healing characteristic, Intelligent Electronic Devices (IED) have to be utilized in the smart grid to comply with protection requirements in the grid. Furthermore, both the traditional network and especially the smart grid are exposed to significant changes in configuration due to the switching of lines, power generations, and bulk consumers.

In order to maintain stability and availability of the power system, the network including all components and devices has to be monitored, and protection and control systems can be updated based on new conditions and system configuration along with the management of power and energy in the system. Hence, the designation of intelligent algorithms and the generation of online computational analysis and design based on the utilization of software and hardware interfaces would be a great advancement for the future of power system protection and control engineering.

INTRODUCTION

The function of protective relaying is to cause the prompt removal from service of any element of a power system when it suffers a short circuit, or when it starts to operate in any abnormal manner that might cause damage or otherwise interfere with the effective operation of the rest of the system.

A practical protective system comprises protective gears like accurate instrument transformers to measure electrical quantities, reliable communication channels for signal transmission, and circuit breakers to isolate the fault from the rest of the network. Besides, microprocessor-based protective relays are fairly capable of recognizing fault conditions and distinguishing faulty areas. In addition, ancillary operators like intelligent algorithms have a significant role in the behaviour of protective relays during abnormal conditions. Maloperation of protective relays in abnormal conditions due to different phenomena has been a serious concern. Many scientific works have investigated the behaviour of protective relays. Ref [1] studies non-fault voltage and current disturbances at the terminals of protective relays. The impact of power quality on protective relaying and power quality monitoring functions in the relays are investigated in [2]. The impact of transient phenomena on the operation of protective relays has also been studied in literature. Transient testing of protective relays like distance, load shedding, and generator protective relays are implemented in [3]. The transient performance of instrument transformers has been analysed in several works. The transient performance of a Rogowski coil is analysed by ATP for protective relay applications in [4].

Ferroresonance is a phenomenon that generally occurs in the distribution network and is significantly probable in high-voltage (HV) systems [5–7]. Sub-Synchronous Resonance (SSR) is a phenomenon in which electrical energy is exchanged between generators and transmission systems below the power frequency [8-12]. The impact of ferroresonance and sub-synchronous resonance on the operation of different kinds of protective relays is investigated in [13, 14]. Adaptation of protective relays against different conditions is discussed in technical literature. Ref [15] presents an adaptive impedance relay with a composite polarizing voltage to enhance the capability against fault resistance. The adaptive out-of-step relay presented in [16] recognizes power system changes and uses a modified system impedance matrix to change relay setting quantities. Furthermore, ref. [17] has developed an algorithm that would set and coordinate the relays in an online mode. In addition to that, several works propose intelligent algorithms for different kinds of protective relays against ferroresonance [18-22]. The algorithms are based on the analysis of ferroresonance in the time domain and the detection of subharmonic frequencies in the network. Nowadays, proliferation of electrical networks requires the application of state-of-the-art protective relays with intelligent algorithms to recognize quasi-fault conditions due to nonlinear abnormalities and respond to fault conditions accurately.

Nowadays, electrical power systems are growing, and distribution networks are increasingly complicated due to the high penetration of renewable energy resources. This causes enormous difficulties respecting the reliability and availability of electricity in the network. The term 'smart grid' is a new definition of a network including power sources, especially renewable energy generations, and consumers. The smart grid urges to enhance the reliability of electricity in the network. To attain this purpose, it provides a bidirectional feature of information among generations and consumers. It also allows the establishment of power flow in different directions due to the distribution of renewable power generations like wind turbines and solar plants [23].

Smart grid comprises several microgrids, which are also able to operate in an islanding mode by the grace of renewable energy resources. In order to distinguish variety forms of faults in a wind farm and protection of DFIG, several methods and algorithms are discussed in technical literature. Ref. [24] utilizes positive and negative measured values to discriminate faults inside or outside of the wind farm. A directional overcurrent element is employed in [25] to protect the generator in a wind farm. Ref. [26] represents a state-of-the-art overcurrent protection based on wide-area measurement in the smart grid. Adaptive algorithms for microprocessor-based distance relays applicable in the smart grid are proposed in.[27]

In addition to that, adaptive protection in the smart grid gains a lot of attention in technical literature. Ref. [28] proposes the mitigation of distributed generation impact on directional overcurrent relay coordination by employing an adaptive protection scheme using a differential evolution algorithm, which causes an improvement in the overall sensitivity of relays. Ref. [29] assesses the requirements for selectivity and sensitivity of an overcurrent relay protection against phase-to-phase faults at the connection of renewable energy sources. Wavelet transform is widely used in the area of protection in the smart grid. Ref. [30] investigates a novel hybrid technique consisting of wavelet packet transform (WPT). In addition, direct and quadrature (dq) axis components are utilized to find out and evaluate the best signature of the internal faults. A new technique for fault classification and detection in the transmission lines of micro-grids using a Discrete Wavelet Transform (DWT) and a Back-Propagation Neural Network (BPNN) is proposed in [31]. Ref. [32] analyses the effectiveness of a wavelet-based protection strategy under dynamic and transient conditions within a micro grid.

Several papers represent new methods of electrical protection in microgrids including wind farms. Ref. [33] presents the simulation and modelling process of an overcurrent protection scheme with pre-established configurations

and centralized control of such configurations. A novel transient current similarity-based protection scheme, which uses the fundamental frequency and non-fundamental frequency characteristics along with transient current, is proposed in [34]. Moreover, a stand-alone Wind Farm Relay (WFR) for collector feeders based on the directional angle algorithm and positive sequence current is introduced in [35]. Renewable energy generations such as wind turbines are particularly vulnerable to ferroresonance and SSR. Ref. [36] analyses ferroresonance in wind turbines in the islanding mode. Influence of ferroresonance in islanding on different kinds of generators in a wind farm is stated in [37]. Ferroresonance in the effect of existing capacitance, which is utilized for VAR compensation in a Wind Park, is expressed in [38]. Analysis of SSR on DFIG and active controls to suppress SSR in a wind farm is explained in [39]. Analysis of Sub-Synchronous Interaction (SSI) between DFIG in a wind farm and the series compensation in the network is presented in [40].

Ref. [41] presents eigenvalue analysis based on the small-signal state-space model of two aggregated direct-drive permanent magnetic synchronous generators (D-PMSGs), which are equivalent to the wind farm. Then, the stability and the SSI between D-PMSGs of the equivalent system can be studied. Ref. [42] presents an SSR assessment framework and tools to more efficiently assess all types of generation in a large system with multiple generators and meshed series capacitors. Ref. [43] reviews DFIG and PMSG with respect to their participation in SSI. Ref. [44] proposes a comprehensive PWM-based modular multilevel converter (MMC) model in both time and frequency domain at the same time. An artificial neural network-based estimator for system identification, which can identify the equivalent transfer function of the whole system in real time, is used in ref. [45]. Ref. [46] deals with the study of ferroresonance events in a distribution grid region characterized by having distributed generators and being lightly loaded. Furthermore, in [47], the guest editorial expresses the necessity of investigation on sub-synchronous interaction and ferroresonance issues in distributed renewable power generations (RPG).

In addition to that, various methods of studying ferroresonance and sub-synchronous resonance and interactions are introduced in several technical works. Ref. [48] presents a comprehensive analysis of sub-synchronous interactions in a wind-integrated power system to understand and mitigate them. Transient and sustained ferroresonance phenomenon in wind farms connected to a power distribution system is studied in [49]. In [50], in order to study the sub-synchronous oscillation in wind power connected to a series-compensated power system and its influencing factors, RT-LAB is used to establish a simulation model concerning wind power connected to a series-compensated power system. The frequency-domain impedance scanning and the time-domain simulation approach are used in [51] to identify and verify sub-synchronous control interaction.

Smart grid mostly insists on a self-healing attribute, which is capable of increasing reliability, preserving voltage magnitude, and improving asset management. Self-healing protection systems take advantage of equipment that recovers the power automatically in case of any abnormality or a fault in the system. Ref. [54] presents a contribution in the area of self-healing distribution networks in the event of a permanent short-circuit. The beneficial aspect of self-healing protection in the smart grid is described in [55]. Self-healing protection comprises any automatic or intelligent system, which recognizes different abnormal conditions, distinguishes the faulty conditions from prevalent phenomena in the network, and makes a suitable decision based on protection strategy to maintain the stability and availability of power in the network. This declines the number of vulnerable consumers in effect of power outages.

In order to enhance the self-healing characteristic of the smart grid, some newly established intelligent protective algorithms are presented in technical literature. An intelligent algorithm based on wavelet transform, neural network, and time domain analysis of ferroresonance is proposed for Negative Sequence Directional Element (NSDE) in [56] to distinguish ferroresonant states and make a decision on the behaviour of the relay in a wind farm. Similarly, ref. [57] proposes an intelligent algorithm based on wavelet transform, neural network, and time domain analysis of ferroresonance for an overcurrent relay in a wind farm. Furthermore, an intelligent algorithm based on subharmonic measurement and ferroresonance analysis is proposed in [58] for a distance relay. The above-mentioned algorithms are able to comply with the smart grid protection strategy. They receive the commands based on the protection strategy to make a suitable decision in ferroresonance and SSR conditions to increase the reliability and availability of electricity in the smart grid.

Consecutive switching of energy resources and microgrid operation modes in the smart grid cause a variety of network configurations. Hence, it requires real-time adaptation of protective systems. Several papers imply on the determination of setting quantities and electrical coordination protection in the smart grid and microgrid. Ref [59] presents a protection system that utilizes extensive communication to monitor the microgrid and update relay fault currents according to the variations in the system. A novel adaptive microgrid protection system using digital relaying based on a centralized architecture and advanced communication is presented in [60]. Ref [61] represents innovative protection methods and devices based on computer relaying techniques. Moreover, some procedures for the coordination and setting of protection relays are suggested. Ref [62] mentions the effects of the distributed generation on the protection coordination and proposes an alternative scheme for protection coordination, using overcurrent relays with pre-set configurations and communicated with microgrid central control unit. In [63], universal protection software based on protection requirements is proposed to design a protective system. The software is applicable in offline and online mode. The online feature updates protective configuration and setting parameters based on changing network configuration by means of a hardware interface.

The above-mentioned history of electrical protection in the presence of nonlinear phenomena and adaptation of protective relays against phenomena like ferroresonance and SSR illustrates a literary insufficiency regarding a complementary reference, which covers all technical aspects of a protective system including a variety of protective

relays, adaptive algorithms, and protection design. The currently published technical works fail to address the need for a comprehensive study that investigates intelligent algorithms compatible for popular kinds of protective relays in both traditional networks and the smart grid. More importantly, though, remarkable resilience from the traditional network to the smart grid urges the technical society in the subject of electrical protection to observe the challenges and put forward innovative ideas to comply with protection strategy requirements in the smart grid.

This book follows previous investigations to propose supplementary materials respecting nonlinear phenomena, especially ferroresonance and SSR, and designates intelligent algorithms for a variety of protective relays in a wide range in traditional networks and smart grid. The occurrence of ferroresonance and SSR is explained along with practical examples in the history of electrical networks in the world. Power oscillation due to ferroresonance and SSR and the interaction between them is analysed in the network. The impact of ferroresonance and SSR on power sources, including renewable power generations, in addition to different types of protective relays, is investigated. Intelligent algorithms against ferroresonance and SSR are designed and examined for protective relays in traditional networks and the smart grid. The characteristics of the algorithms are fairly compatible with the protection strategy requirements in the grid. This book utilizes PSCAD/EMTDC transient analysis software to simulate the above-mentioned phenomena, analyse the behaviours of power generations and protective relays due to the occurrence of phenomena, and carry out the implementation and examination of the proposed algorithms. Moreover, the MATLAB software is utilized to perform Discrete Wavelet Transform and Neural Network analysis and also somewhere is used to plot waveform diagrams, which are obtained from PSCAD/EMTDC simulation results.

In addition to that, this book proposes a power automation system called Universal Protection, Control and Power, Energy Management Centre (UPCPEMC). The centre comprises new simulation, analysis, protection, control, and power system component design software, in addition to power and energy management programs, which are applicable for both traditional networks and the smart grid. However, the application of the software is more efficient in the smart grid as the functionalities of the centre and designated software improve with enhancement of measurement and signal transmission through communication protocol based on SCADA in the grid. The program controls and manages the dispatching of power and energy in the grid including the area under control. The centre utilizes intelligent power and energy management programs, which adapt consumer demand with the capability of power generation of the grid. In addition to that, an appropriate protective system is designed for the grid based on the results of electrical studies and consideration of protective design criteria.

Moreover, the optimum quantities of parameters of control systems in the power network are determined by the software in the centre to increase the reliability of the power system. Furthermore, using the results of electrical studies, the software is able to calculate and determine the technical specification of the components in the grid. The final aim of the centre is maintaining the stability and availability of the power system to supply the consumers efficiently.

Finally, it should be gently stated that this book is an efficient collection of several years' investigations into the matter of intelligent algorithms against nonlinearities and the promotion of new findings in this regard. As the book gives detailed information on the production of protective algorithms and software solutions for protective systems, relay manufacturers, engineering software manufacturers, protective engineers, and service providers of the power system are the most addressees of this book. Hope the book enlightens a way to protect and control the future of power electricity intellectually".

1

THEORETICAL APPROACH

Prior to investigating the impact of nonlinearities on the operation of protective relays and the design and implementation of intelligent algorithms for protective relays, it is essential to review the fundamentals of protective relays operations and specifications, as well as some electrical phenomena that cause maloperation of protective relays. The book focuses on the impact of ferroresonance and SSR on the operation of protective relays. Therefore, in this section, theoretical aspects of ferroresonance, power swing, out of step, and sub-synchronous resonance are explained. Furthermore, the basic principle of prevalent protective relays is described.

1-1- Electrical phenomena

Electrical networks comprise a variety of active and passive elements with linear and nonlinear characteristics, leading to the emergence of various electrical phenomena depending on the elements' characteristics and initial conditions. Ferroresonance and sub-synchronous resonance are nonlinear phenomena that occur in electrical networks in practice.

1-1-1- Ferroresonance

Ferroresonance is a nonlinear resonance that occurs in the presence of a saturated nonlinear inductance and a capacitor in a low-resistance circuit. In a ferroresonance condition, the capacitance line traverses across the nonlinear area of the inductance characteristic, causing the presence of a large magnitude of voltage, current, and frequency deviation in the circuit. The calculation of parameters of nonlinear circuits in the time domain obtains a graphical approach as shown in Fig. 1.2. The inductor voltage of a typical series RLC circuit (Fig. 1.1) is calculated as follows [1]:

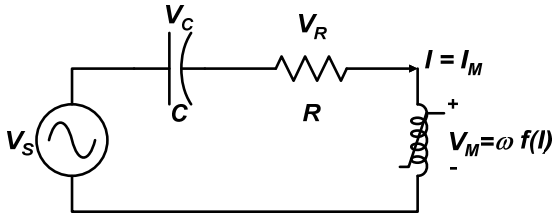

Fig.1.1: Series RLC Ferroresonant circuit example

$$V_M = \sqrt{V_S^2 - (I.R)^2} + \frac{I}{\omega C} \tag{1.1}$$

where:
V_S is the total voltage across the circuit.
V_M is also a nonlinear function of current as follows:

$$V_M = \omega f(I) \tag{1.2}$$

The voltage across the reactance in the circuit is presented as follows:

$$V_M = X_M I_M \tag{1.3}$$

In this example, the inductance is a nonlinear element in effect of the core saturation & hysteresis. The voltage across the capacitor in the circuit is presented as fallows.:

$$V_C = X_C I_M \tag{1.4}$$

Similarly, by elimination of the effect of resistance, the voltage across the inductance can also be expressed as follows:

$$V_M = V_S + (X_C I_M) \tag{1.5}$$

The equations (1-3) and (1-5) plotted in Fig. 1.2 illustrate three possible 60 Hz steady-state operating points for positive values of voltage and current. Points 1 and 2 are stable operating points; whereas point 3 is unstable. Stability of the operating points can be specified mathematically through further analysis explained as follows.

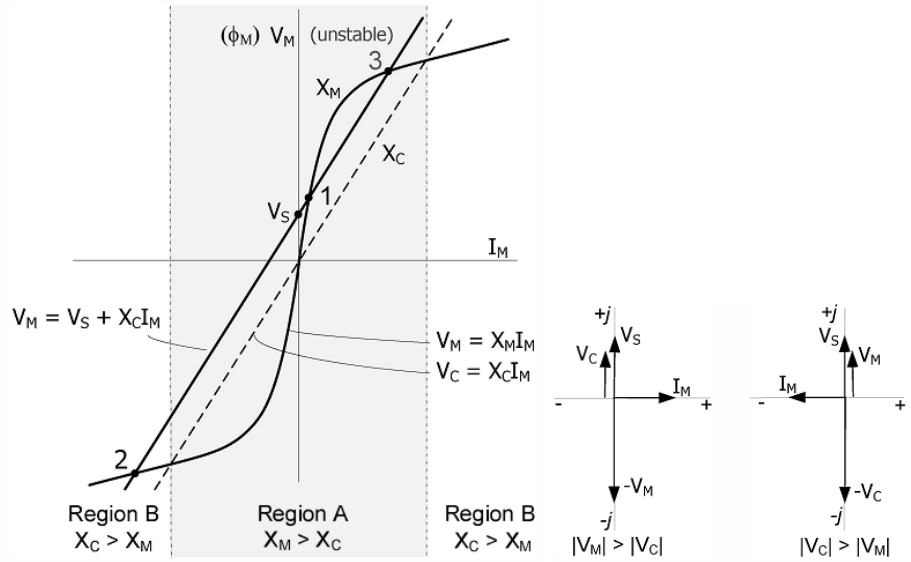

a b

Fig. 1.2: Graphical analysis of series RLC circuit with a nonlinear inductor, a) operating characteristic diagram, b) phasor diagram

As shown in Fig. 1.2a, the value (slope) of XM is greater than Xc (shown as the dashed line) in region A. This causes the current IM to lag with respect to the source voltage Vs. The phasor diagram for this region is shown in Fig. 1.2b where |V_M |>|V_C |. In the circuit of fig. 1.1, this illustrates that for the loop voltage summation the following equation must be fulfilled.

$$V_S + V_C + V_M = 0 \tag{1.6}$$

To fulfil equation (1.6), VM acts in opposition to source voltage Vs and VC acts in the direction of Vs. Whereas, the magnitude of Xc is greater than XM in region B. This causes the current IM to lead with respect to the source voltage VS. That is to say, IM is now negative with respect to the previous lagging value. This shows that VM acts in the direction of the source voltage Vs and VC acts in opposition to Vs to fulfil equation.(1.6)

At point 1, situated in region A, a small increase in current causes an increase in VM greater than VC as XM has a larger slope. Hence, the difference of VM-VC is inductive and behaves in opposition to Vs. The circuit impedance increases enforcing a reduction in current so that the current returns to the intersection. Conversely, in case of a small decrease in current, VM decreases more sharply than VC and the difference of VM-VC becomes less inductive and still behaves in opposition to Vs, though less than before. The circuit impedance decreases enforcing an increase in current so that the current returns to the intersection. Consequently, operating point 1 is considered stable because small changes in current or voltage are not able to change the operating point. However, a significant change (a transient) in current or voltage operation can move operating point 1.

At point 2, situated in region B, a small increase in current causes an increase in VC more than VM as XC has a larger slope. Hence, the difference of VM-VC is capacitive and behaves in opposition to Vs. The circuit impedance (capacitive reactance) increases enforcing a reduction in current so that the current returns to the intersection. Conversely, in case of a small decrease in current, VC decreases more sharply than VM and the difference of VM-VC becomes less capacitive and still behaves in opposition to Vs, though less than before. The circuit impedance (capacitive reactance) decreases enforcing an increase in current so that the current returns to the intersection. Consequently, operating point 2 is considered stable because small changes in current or voltage are not able to change the operating point. However, a significant change (a transient) in current or voltage operation can move operating point 2.

At point 3, situated in region A, a small increase in current causes an increase in VC more than VM as XC has a larger slope. Hence, the difference of VM-VC is capacitive and behaves in the direction of Vs. The circuit impedance decreases resulting in an increase of current and an increase in the voltage away from the intersection. As the voltage increases, the current continues to increase and so on. Conversely, in case of a small decrease in current, VC decreases more sharply than VM and the difference of VM-VC becomes inductive and behaves in opposition to Vs. The circuit impedance increases enforcing a decrease in current away from the intersection. Consequently, operating point 3 is considered unstable because small changes in current or voltage easily change the operating point.

As shown in Fig. 1.3, the intersection of VM = ωf(I) and VC represents the operating point of the circuit. Variation in capacitance of the circuit analogously causes a change in the slope of the characteristic given by tanα = 1/ ωC. On

the other hand, variation in inductance leads to an interaction with a wide range of capacitances leading to emerging several stable steady state responses to any given change of parameters. It causes changes in the configuration of the circuit so the capacitance line crosses the nonlinear area of the VM = ωf(I) curve, resulting in the occurrence of ferroresonance in the circuit.

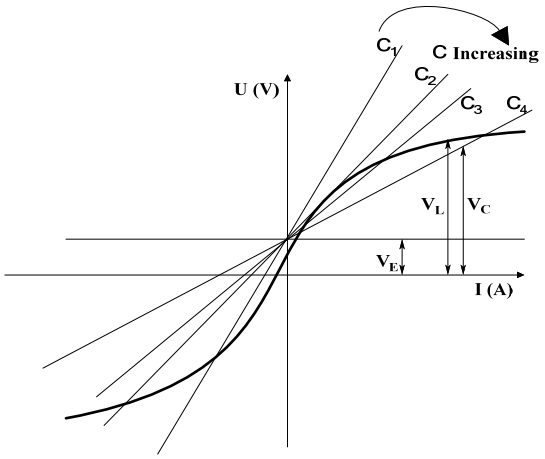

Fig. 1.3: Operating characteristics of Series RLC Ferroresonant circuit

Fig. 1.4 shows the graphical solution, which considers the impact of resistance in ferroresonance. To achieve this purpose, equation (1.1) is used as it has been developed from Kirchhoff's Law by summing the voltage drops around the series circuit. Equation (1.1) is an ellipse that is symmetrical about the slope Xc.

Plotting equation (1.1) in Fig. 1.4 shows three intersections, where points 1, 2, and 3 represent solutions for values of Vs. Point 1 represents the normal operating state, point 2 represents the ferroresonant state, and operation at point 3 is unstable and may not occur. The ellipse contracts with increasing R, illustrating the possibility of eliminating ferroresonance at point 2 with sufficient loading. Therefore, point 1 would be the only possible operating point, which is definitely situated in the linear area of the characteristic. The ellipse expands with decreasing R, so if R is equal to zero, then equation (1.1) is reduced to equation (1.4). Consequently, two straight lines on Fig. 1.4 are identified as R = 0.

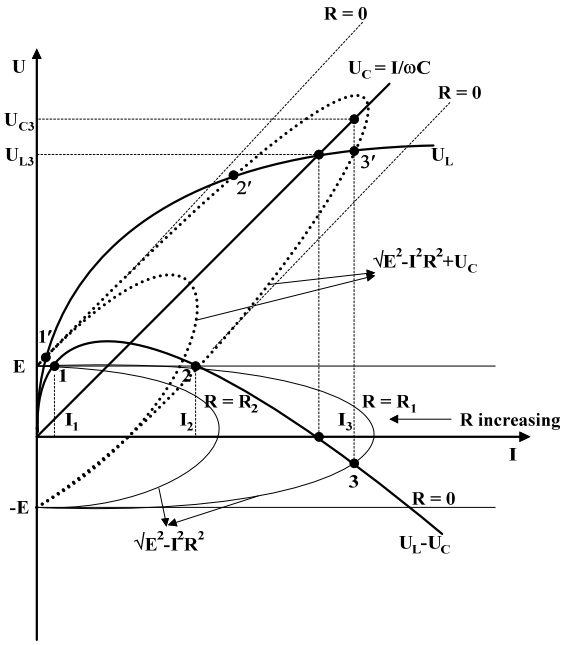

Fig. 1.4: Graphical solution for consideration of resistance in ferroresonance

As mentioned earlier, the frequency of the waveform can deviate from the nominal frequency in ferroresonance. This frequency deviation can be determined as follows [3]:

$$\Delta f = |f_{fr} - f_{nom}| \tag{1.5}$$

where:
f_{fr} = frequency of the waveform in ferroresonance

As shown in Fig. 1.5a, the frequency of the voltage waveform is a function of nT period in subharmonic ferroresonance (where n is an integer). The harmonic spectrum of subharmonic ferroresonance with an integer number of harmonics is shown in Fig. 1.5b. It must be noted that f_{fr} is calculated based on the number of zero crossings of the waveform in one second in non-periodic ferroresonance.

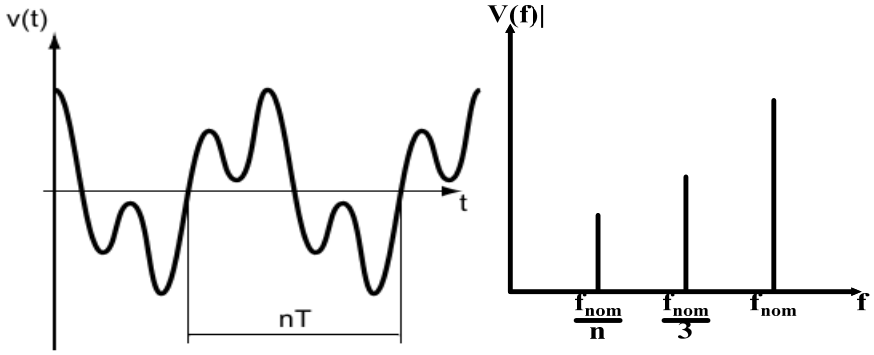

Fig. 1.5: Characteristic of sub harmonic ferroresonance, a) Electrical waveform, b) Harmonic spectrum

Deviated waveforms as a result of ferroresonance are decomposed into a number of harmonics using FFT (Fast Fourier Transform). Measurements are based on the evaluation of samples, which are taken at specific intervals. Therefore, Discrete Fourier Transform (DFT) is used with a particular sampling rate to illustrate the harmonic components on the harmonic spectrum.

$$V_{Lk} = \sum_{n=0}^{N-1} V_{Ln} e^{-j2\pi k\frac{n}{N}} \qquad K = 0 \dots N-1 \qquad (1.6)$$

N = number of samples

Total Harmonic Distortion (THD) is calculated based on integer harmonics, which are attained from the FFT. They are considered in the following formula:

$$THD = \sqrt{\sum_{h=2}^{x} \left(\frac{\text{individual (h)}}{\text{individual (1)}}\right)^2} \qquad (1.7)$$

x = integer harmonics

In order to determine different types of ferroresonance based on measurements in a logical manner, ferroresonant characteristics must be quantified. The values of THD and Δf are used as criteria to distinguish different types of ferroresonance. Table 1.1 categorizes the different types of ferroresonance.

Table 1.1: Criteria to determine Ferroresonance modes

Ferroresonance type	Δf (Hz)	dΔf/dt (Hz/S)	T.H.D (%)	Harmonic spectrum
Fundamental	< 1	≈ Zero	> 50	Discrete
Harmonic	> 1	> 5	> 70	Discrete
Quasi-periodic	variable	> 10	> 100	Discrete
Chaotic	variable	> 15	> 120	Continuous

The quantities of criteria stated in Table 1.1 are typical and may vary in different applications. The table shows that fundamental ferroresonance is recognized when the waveform frequency is at the nominal value and Δf is less than 1 Hz, with dΔf/dt (calculated based on equation 1.8) close to zero, and a THD value greater than 50%.

$$\frac{d\Delta f}{dt} = T.\frac{\Delta f(t) - \Delta f(t-\Delta t)}{\Delta t} \qquad (1.8)$$

where:
T = time constant
$t - \Delta t$ = previous time step
Δt = time step interval

In the case of deviation of waveform frequency from the nominal value, harmonic ferroresonance is detected when Δf is higher than 1 Hz, dΔf/dt is higher than 5 Hz/s, and THD value is more than 70%. Fundamental and harmonic ferroresonance often include odd harmonics, resulting in a mostly discrete harmonic spectrum. Quasi-periodic ferroresonance is detected similarly, with variable Δf values, dΔf/dt higher than 10 Hz/s, and THD more than 100%.

Chaotic mode is detected with variable Δf values, dΔf/dt higher than 15 Hz/s, and THD more than 120%. The main difference between quasi-periodic and chaotic modes is that quasi-periodic contains a discrete harmonic spectrum, while chaotic mode has a continuous harmonic spectrum. In these situations, the THD can exceed 100%, indicating a chaotic mode with a continuous harmonic spectrum. The recognition of continuous or discrete harmonic spectrum is a visual characteristic, where THD and Δf are primarily used to determine ferroresonance modes.

1-1-2- Power swing and out of step condition

The power network connects power generation to load through transmission lines, operating at a nominal frequency and maintaining a voltage difference of about 5% between buses in steady-state conditions. In a power network with a nominal frequency of 60 Hz, power frequency typically deviates within a range of about +/- 0.02 Hz. In steady-state operating conditions, the balance between generated and consumed active and reactive powers leads to a dynamic change in power flow when equilibrium is established between generation, load, and transmission. These power flow variations are compensated for automatically by control systems such as governors and exciters, and have no detrimental impact on the power network or protective systems.

1-1-2-1- Stability analysis

To conduct stability analysis in a power system with rotary generation, the swing equation (1.9) is used. The Swing Equation of generator describes the relative motion between the rotor axis and the synchronously rotating stator filed axis with respect to time. Under normal operating conditions, the relative position of the rotor axis and the resultant magnetic field axis is fixed. The angle between the two is known as the power angle or torque angle. During any disturbance, the rotor decelerates or accelerates with respect to the synchronously rotating air gap magneto-motive force, creating relative motion. The equation describing the relative motion is a non-linear second order differential equation that describes the swing of the rotor of synchronous machine. The power exchange between the mechanical rotor and the electrical grid due to the rotor swing (acceleration and deceleration) is called inertial response. The swing equation describes the behaviour of the rotor dynamics. The torque angle δ is the angle of the internal EMF of the generator and it dictates the amount of power that can be transferred [4, 5]. This angle is therefore called the load angle. By solving the equation (1.9) including specific values of H, in addition, mechanical and electrical power, the rate of change of load angle and subsequently speed variation of the machine is obtained.

$$\frac{d^2\delta}{dt^2} = \frac{\omega_s}{H}(P_m - P_{e)} \tag{1.9}$$

where:
H (S) = Inertia constant of the machine
P_m (MW) = Mechanical power of the machine
P_e (MW) = Electrical power of the machine
δ (degree) = Load angle

The equal area criterion is a method for determining transient stability of two-machine systems or a single machine against an infinite bus, using a graphical approach. This principle does not require the swing equation for the determination of stability conditions. Fig. 1.6a shows the correlation between stable and unstable power swing according to variation of rotor angle. In stable swing, the rate of dδ/dt remains restricted in a specific time and load angle is limited to δ_{max}. While, in unstable swing, the rate of dδ/dt has increasing manner for a long time and load angle exceeds δ_{max}. According to equal area criterion shown in Fig. 1.6b, if the rotor's acceleration area A_1 during the fault is equal to its maximum possible deceleration area A_2 after the fault is removed, the system is in the transient stability critical state as expressed by the following formula:

$$A_1 = \int_{\delta_0}^{\delta_c}(P_m - P_e)\,d\delta = A_2 = \int_{\delta_c}^{\delta_m}(P_e - P_m)\,d\delta \tag{1.10}$$

Angle δ_c is considered as critical angle so that in the angle larger than this value, the system would be unstable. To be clearer, the maximum allowable value of the clearing angle δ_c and clearing time t_c for the system to remove the disturbance without interrupting the system's performance and remain stable are known as critical clearing angle and critical clearing time (CCT) respectively [5].

$$\delta_c = \frac{\pi f_0 P_0}{2H}(\delta_c - \delta_0) \tag{1.11}$$

$$t_c = \sqrt{\frac{2H}{\pi f_0 P_0}(\delta_c - \delta_0)} \tag{1.12}$$

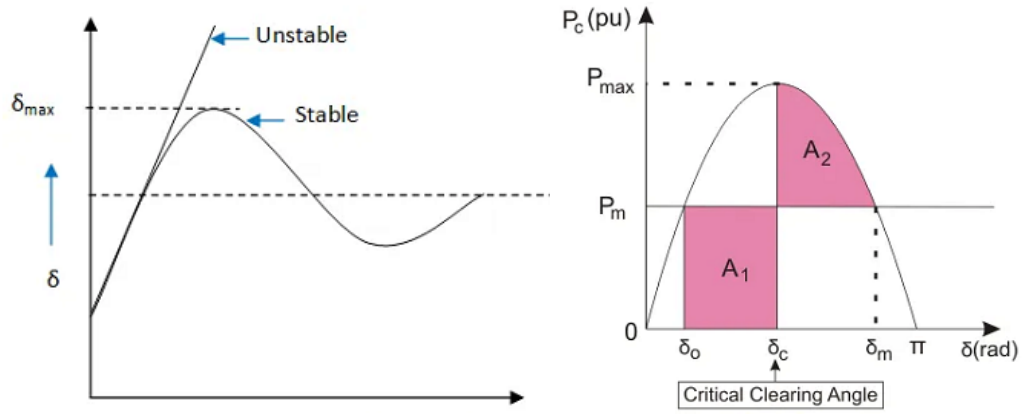

Fig. 1.6: a) presentation of swing stability, b) presentation of equal area criterion

1-1-2-2- Power swing measured by protective system

Fig. 1.7 shows a simplified system diagram of two generating sources [6]. During a system out of step (OOS) condition, the protective system may detect the OOS as a phase fault if the trajectory enters the operating characteristic of pole slipping function in the generation plant or distance relay in the substation. To demonstrate this, let us look at the impedance that the relay measures during an OOS condition for the simple two-source system.

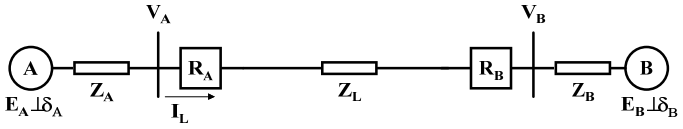

Fig. 1.7: simplified diagram of a two-machine system

As shown by Fig. 1.6, the current IL at relay R_A is computed as follows:

$$I_L = \frac{E_A - E_B}{Z_A + Z_L + Z_B} \tag{1.13}$$

The direction of current flow remains unchanged during the power swing event. In fact, the voltages of both sides change with respect to each another. The impedance measured at the relay R_A is calculated as follows:

$$Z_{RA} = \frac{V_A}{I_L} = \frac{E_A - I_L Z_A}{I_L} = \frac{E_A}{I_L} - Z_A = \frac{E_A(Z_A + Z_L + Z_B)}{E_A - E_B} - Z_A \tag{1.14}$$

In the system diagram of Fig. 1.7, it is assumed that E_A has a phase advance of δ over E_B where $\delta = \delta_A - \delta_B$ and the ratio of two source voltages is $n = \frac{E_A}{E_B}$ then, we have:

$$\frac{E_A}{E_A - E_B} = \frac{n(\cos\delta + j\sin\delta)}{n(\cos\delta + j\sin\delta) - 1} = \frac{n[(n - \cos\delta) - j\sin\delta]}{n - \cos\delta^2 + \sin^2\delta} \tag{1.15}$$

In case the two sources magnitude of voltages is equal or n = 1, equation (1.15) is stated as:

$$\frac{E_A}{E_A - E_B} = \frac{1}{2}(1 - j\cot\frac{\delta}{2}) \tag{1.16}$$

Finally, the impedance measured at the relay R_A is calculated as below:

$$Z_{RA} = \frac{V_A}{I_L} = \frac{(Z_A + Z_L + Z_B)}{2}(1 - j\cot\frac{\delta}{2}) - Z_A \tag{1.17}$$

Furthermore, in terms of power oscillations and fluctuations in the network, some basic definitions are considered, like power swing, out of step, and pole slipping. Power swing is basically a variation in power flow that occurs whenever the internal voltage of a generator or group of generators at one location of the power system slips with respect to a generator or group of generators at another location due to oscillation of the rotor angle of the machines. In other words, the swing occurs whenever the generator rotor angles are advancing or retarding with respect to each other in response to changes in load magnitude and direction, line switching, loss of generation, faults, and other system disturbances.

Depending on the stability characteristic of the oscillation, power swing is regarded as stable or unstable. In stable power swing, the generators do not experience pole slipping. Pole slipping is a condition in a power system where a generator or group of generators' terminal voltage angles (load angle) traverse over 180 degrees with respect to the rest of the connected power system. In stable power swing, the terminal voltage angle of the machine does not pass 180° with respect to the power system voltage. As shown in Fig. 1.8, δ2 is considered a stable load angle. In a stable power swing, the operating point does not traverse across the vertical border X and go back towards the normal operating point (δ1), and the system reaches a new state of equilibrium and an acceptable operating condition. According to stability studies and technical experiences, stable swings are swings that go back to a normal state before they experience a load angle of 120°[7].

An unstable power swing, also known as an out-of-step condition, is a power swing that causes a generator or group of generators to experience pole slipping. In Fig. 1.8, δ3 is considered an unstable load angle. The electrical system centre or voltage zero is the point or points in the system where the voltage becomes zero during an unstable power swing.

The trajectory of the measured impedance at the relay during a power swing when the angle between the two source voltages varies corresponds to the straight line that intersects the segment A to B at its middle point. This point is called the electrical centre of the swing. The angle between the two segments that connect P to points A and B is equal to the angle δ, where the angle equal to δ1 is considered the normal operating point. In the case of n = 1, a circular impedance trajectory with an infinite radius traverses towards the electrical centre. When the angle δ reaches the value of 180 degrees, the impedance is precisely at the location of the electrical centre. It can be observed that the impedance trajectory during a power swing traverse across any relay characteristic, which is situated in the impedance of the system [6].

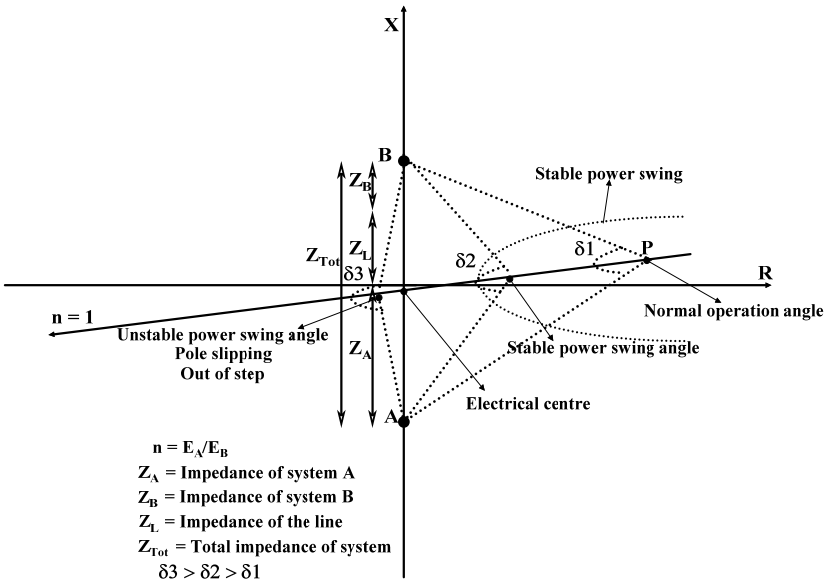

Fig. 1.8: Phasor diagram respecting occurrence of power swing in the network

As can be inferred from what is mentioned above, the shape and characteristics of the impedance trajectory depend on the ratio of n = EA/EB. In case of n > 1, a circular impedance trajectory traverses across the area with positive reactive power; whereas, in case of n < 1, a circular impedance trajectory traverses across the area with negative reactive power. The ratio of n and total impedance determines the diameter and centre of the circles. For a specific total impedance, increasing n above 1 causes the diameter to decrease, and the centre of the circle moves away from the origin towards the area with positive reactive power. As shown in Fig. 1.9a, the centre of the circle from point B is determined by equation (1.18), and the radius of the circle is calculated by equation (1.19):

$$C_{(n>1)} = \frac{Z_{Tot}}{n^2-1} \tag{1.18}$$

$$R_{(n>1)} = \frac{nZ_{Tot}}{n^2-1} \tag{1.19}$$

Similarly, decreasing n under 1 causes the diameter to decrease and the centre of the circle moves away from the origin towards the area with negative reactive power. As shown in Fig. 1.9b, the centre of the circle from point A is determined by equation (1.20), and the radius of the circle is calculated by equation (1.21) [8]:

$$C_{(n<1)} = \frac{n^2 Z_{Tot}}{1-n^2} \tag{1.20}$$

$$R_{(n<1)} = \frac{nZ_{Tot}}{1-n^2} \tag{1.21}$$

The time to traverse the impedance trajectory in the impedance diagram is calculated by consideration of two points on the scheme. For instance, points C and D correspond to δ2 and δ3 in Fig. 1.9a. The time to traverse the distance between C and D is calculated by the following formula:

$$t = \frac{\delta 3 - \delta 2}{S} \tag{1.22}$$

where:
S = slip in Degrees/second

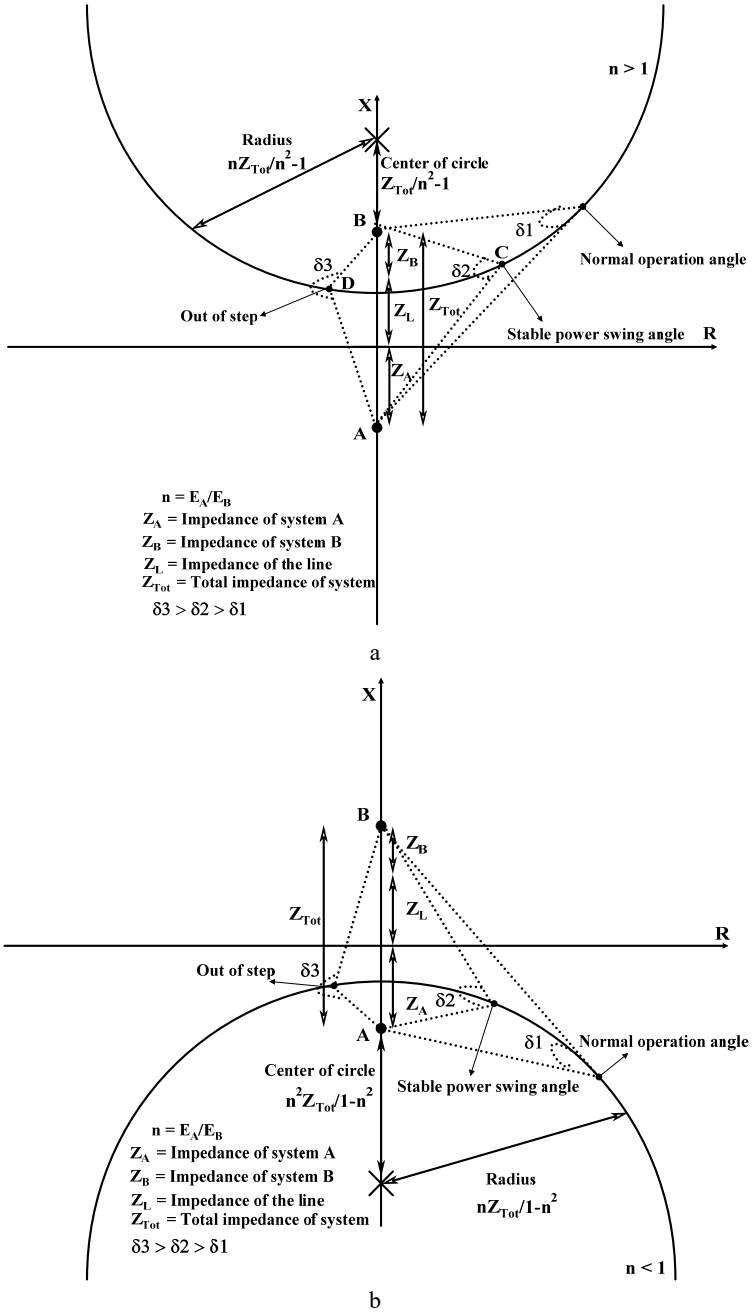

Fig. 1.9: Phasor diagram respecting occurrence of power swing, a) n > 1, b) n < 1

Fig. 1.10 shows the impedance characteristic with different values of n, and load angle. Increasing the ratio of n more than 1 causes decreasing the diameter and centre of the circle move away from the origin towards the area with positive reactive power. Reciprocally, decreasing the ratio of n less than 1 causes decreasing the diameter and centre of the circle move away from the origin towards the area with negative reactive power. The angle drawn between the two points A and B is equal to the load angle δ. In this way, for instance, all the impedance locations in circumference

of the circle specified by δ1 have the same load angle regardless of whether the ratio of n is equal, more than or less than 1.

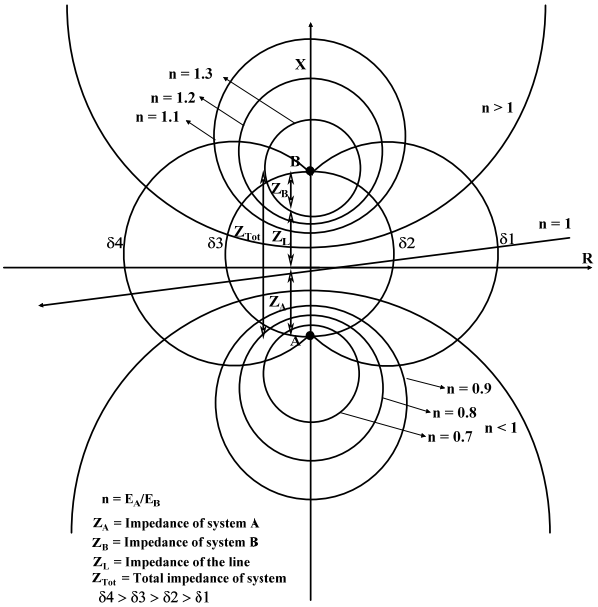

Fig. 1.10: Phasor diagram respecting different values of n, and load angle

As was discussed in advance, sudden fluctuations in electrical power network are resulted by power system faults, switching operation, and generator disconnection, loss of excitation, and loss or application of large amount of load. While the mechanical power input to generators remains proportionally constant. Such disturbances bring about oscillations in machine rotor angles so the rotor angles become advancing or retarding relative to each other and consequently result in severe power swing in the network. It must be noted that, advancing or retarding load angle in power swing depends on increasing or decreasing, respectively, mechanical power with respect to electrical power. For instance, in case of increasing mechanical power more than electrical power, the load angle increases and impedance trajectory moves towards the left hand of the impedance diagram and is considered as advanced power swing as was shown in Fig. 1.8 and 1.9.

Reciprocally, in case of increasing electrical power more than mechanical power, the load angle decreases and impedance trajectory moves towards the right hand of the impedance diagram and is considered as retarded power swing as shown in Fig. 1.11. In retarded power swing, the machine is changed from generator operation to motor operation mode (generator motoring). The load angle becomes negative and impedance trajectory moves counter clockwise. As shown by the graph, in load angle δ3, impedance trajectory passes through 180°, which means that out of step occurs in the system.

Thereafter, the impedance goes back to origin in a circulating circuit, considering accomplishment of one cycle of slip frequency. The impedance enters to the left side of protective relay characteristic, which may be installed between system A and B. entering the impedance trajectory to the protective characteristic from the left side warn the relay regarding occurrence of retarded power swing. Unstable retarded power swing causes relay operation at different locations in the network. Unexpected out of step can exacerbate the power system disturbance and leads in extensive power outage or entire blackout.

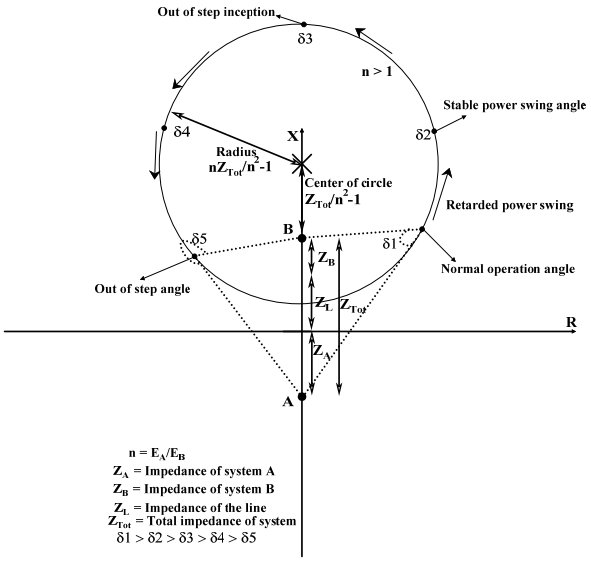

Fig. 1.11: Phasor diagram respecting occurrence of retarded power swing in the network

Variation of load angle in an out-of-step condition causes a phase difference between the voltage of the generator and grid voltage. The phase difference leads to an increase in the magnitude of the voltage, reaching a maximum of up to 2Vm across the circuit breaker, which is responsible for separating the generator from the network in a phase difference of 180°. Additionally, the opening of the circuit breaker is accompanied by Transient Recovery Voltage (TRV), which is the voltage that appears across electrical equipment like circuit breakers shortly after a current interruption.

The waveform of the recovery voltage, including the magnitude and frequency, actually depends on the circuit configuration (inductive, resistive, or capacitive nature) and is a critical parameter for fault interruption by a high-voltage circuit breaker. Depending on the characteristics of TRV, such as amplitude and rate of rise, the breaker operation can either lead to a successful current interruption or a failure (reignition or restrike).

In fact, the TRV is a high-frequency waveform that is superimposed on the voltage waveform while opening the circuit breaker. The frequency of the TRV is called the natural resonance frequency (fnr), which is dependent on the R-L-C characteristics of the system connected to both terminals of the circuit breaker and is formulated as follows:

$$f_{nr} = \frac{1}{2\pi\sqrt{LC}} \text{ (Hz)} \tag{1.23}$$

The characteristics of the TRV waveform also depend on the type of fault that the breaker has to interrupt, such as single, double, or three-phase faults, grounded or ungrounded faults. Furthermore, it depends on the characteristics of the system, including the type of neutral connection (effectively grounded, ungrounded, solidly grounded) and the type of load (capacitive, inductive, resistive), as well as the type of connection (cable connected or line connected). The rate of rise of the voltage across the circuit breaker is a function of the surge impedance of the system and is calculated as follows:

$$R_{bo} = 1.5\sqrt{2}\,\omega IZ \text{ (kV/μs)} \tag{1.24}$$

where:
I = current of the system at the instance of opening circuit breaker
Z = surge impedance of the system

The value of the maximum voltage in a system including several parallel lines connected to a common bus bar is calculated as follows:

$$E = 800IL_s\left(1 + \frac{2}{n}\right) \text{ (kV)} \tag{1.25}$$

where:
Ls = bus inductance
n = number of transmission lines with the same surge impedance connected to the bus

More information regarding TRV in circuit breakers can be found in [9, 10]. In addition to that, several works discuss the measurement of switching over voltages at substations and on transmission lines in extra-high-voltage systems, as well as the impact of transient over voltages on the power system[13 ,11] .

In order to present the theoretical aspects of TRV, we decided to simulate a switching operation in an out-of-step scenario. Fig. 1.12 shows an out-of-step condition in a two-machine system implemented in PSCAD/EMTDC software to illustrate swing characteristics and TRV while opening a circuit breaker. The frequency difference between the two power sources is 1 Hz, causing a slip frequency of 1 Hz in the network. Fig. 1.12a shows the disconnection of the circuit breaker at 3 seconds from the beginning of the simulation, where the phase angle difference between the two systems is zero in the power swing trajectory. In such a situation, the TRV, in addition to the voltage difference across the breaker, is zero at the instance of the breaker operation. Subsequently, the voltage difference across the breaker reaches a maximum value of about 400 kV peak during a period of 0.5 seconds according to the slip frequency of 1 Hz.

Fig. 1.12b shows the disconnection of the circuit breaker at 3.5 seconds from the beginning of the simulation, where the phase angle difference between the two systems is 180° in the power swing trajectory. In this situation, the TRV emerges with a magnitude of approximately 119 kV peak, which is superimposed on the voltage difference of about 2Vm = 400 kV peak across the breaker, consequently causing a voltage difference of about 519 kV peak at the instance of the breaker operation. It can be observed from the graph that the magnitude of the voltages at the stations increases from 200 kV peak to nearly 260 kV peak and 259 kV peak respectively in transient time during the switching operation in opposite directions, justifying the increment of the TRV to a value of 60 + 59 = 119 kV peak.

Fig. 1.12c shows a closer view of the switching operation at 3.5 seconds from the beginning of the simulation, where the phase angle difference between the two stations is 180° as explained previously. Fig. 1.12d shows a close view of the switching operation at 3.75 seconds from the beginning of the simulation, where the phase angle difference between the two stations is far from 180° and passes throughout the electrical centre of the system. According to a slip frequency of about 1 Hz, it is expected that at the aforementioned time of the simulation, the breaker opens the circuit with a phase angle difference of about 90°. In this situation, the magnitude of the voltage across the breaker, excluding TRV, is 1.5Vm.

As shown in the graph, the phase angle difference experiences fluctuations, which follow TRV oscillations and cause a transient increment of the angle up to 109°, then suppressed to 86°. Consequently, the resulting magnitude of the voltage across the breaker increases up to 395 kV peak, including TRV in transient time. This voltage increment is tolerable for the breaker to open the circuit successfully. Hence, as shown in Fig. 1.13, in order to facilitate the open operation of a circuit breaker in an out-of-phase condition, the protective relay issues a trip operation to the breaker typically at the load angle of 270°; this means a phase angle difference of about 90°.

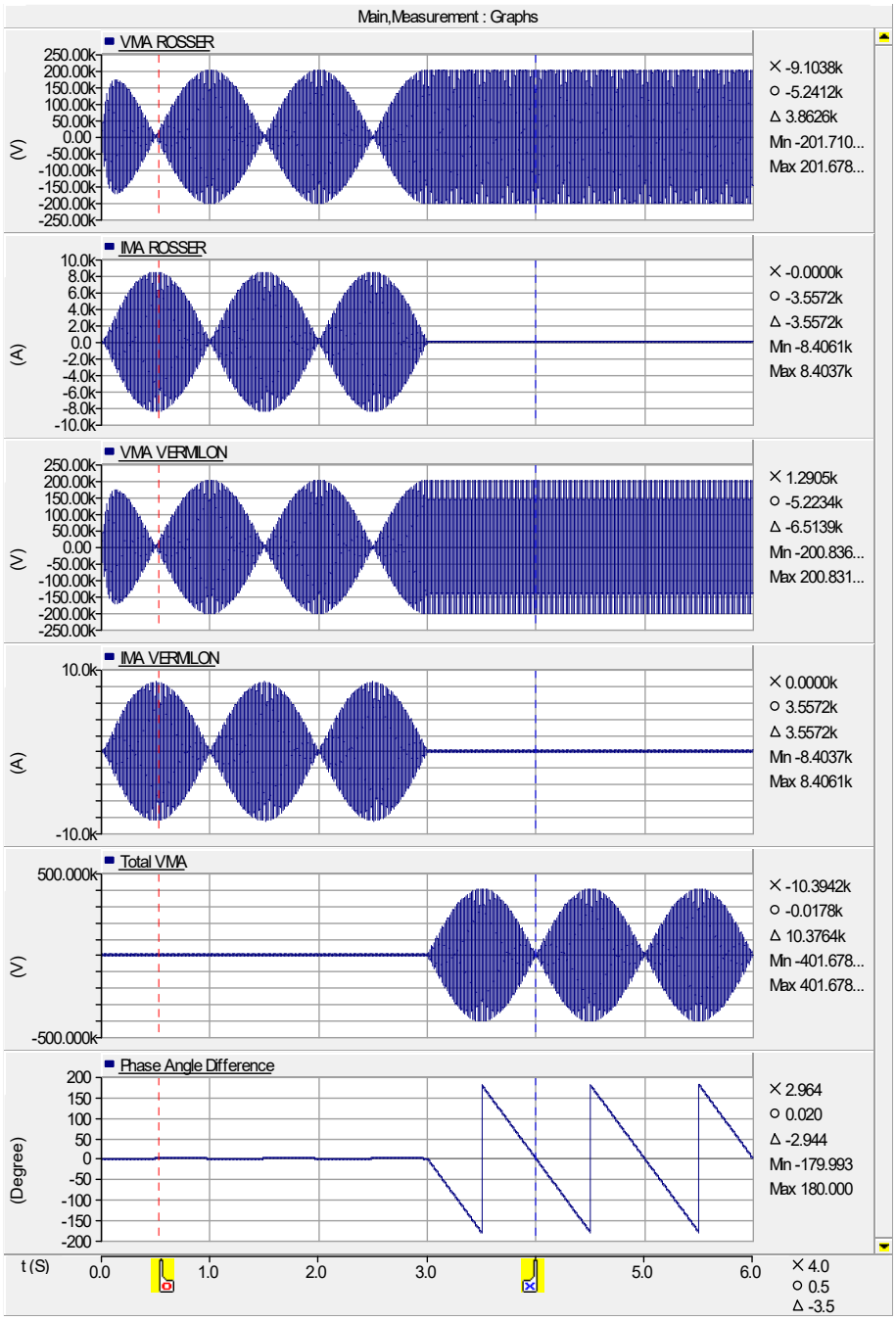
Main,Measurement : Graphs
VMA ROSSER
250.00k
200.00k
150.00k
100.00k
50.00k
0.00
-50.00k
-100.00k
-150.00k
-200.00k
-250.00k
(V)
X -9.1038k
O -5.2412k
Δ 3.8626k
Min -201.710...
Max 201.678...
IMA ROSSER
10.0k
8.0k
6.0k
4.0k
2.0k
0.0
-2.0k
-4.0k
-6.0k
-8.0k
-10.0k
(A)
X -0.0000k
O -3.5572k
Δ -3.5572k
Min -8.4061k
Max 8.4037k
VMA VERMILON
250.00k
200.00k
150.00k
100.00k
50.00k
0.00
-50.00k
-100.00k
-150.00k
-200.00k
-250.00k
(V)
X 1.2905k
O -5.2234k
Δ -6.5139k
Min -200.836...
Max 200.831...
IMA VERMILON
10.0k
-10.0k
(A)
X 0.0000k
O 3.5572k
Δ 3.5572k
Min -8.4037k
Max 8.4061k
Total VMA
500.000k
-500.000k
(V)
X -10.3942k
O -0.0178k
Δ 10.3764k
Min -401.678...
Max 401.678...
Phase Angle Difference
200
150
100
50
0
-50
-100
-150
-200
(Degree)
X 2.964
O 0.020
Δ -2.944
Min -179.993
Max 180.000
t (S)
0.0
1.0
2.0
3.0
5.0
6.0
X 4.0
O 0.5
Δ -3.5

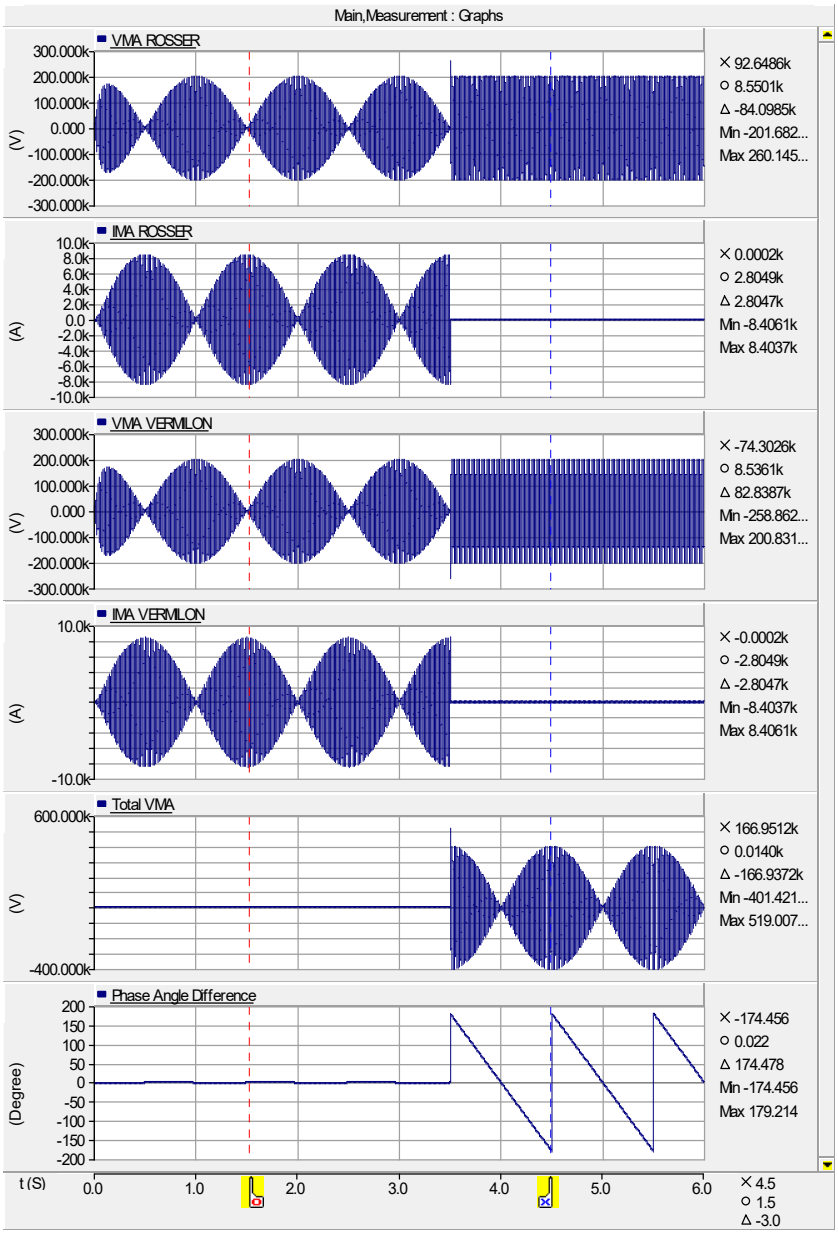
Main,Measurement : Graphs
VMA ROSSER
(V)
300.000k
200.000k
100.000k
0.000
-100.000k
-200.000k
-300.000k
× 92.6486k
○ 8.5501k
Δ -84.0985k
Min -201.682...
Max 260.145...
IMA ROSSER
(A)
10.0k
8.0k
6.0k
4.0k
2.0k
0.0
-2.0k
-4.0k
-6.0k
-8.0k
-10.0k
× 0.0002k
○ 2.8049k
Δ 2.8047k
Min -8.4061k
Max 8.4037k
VMA VERMILON
(V)
300.000k
200.000k
100.000k
0.000
-100.000k
-200.000k
-300.000k
× -74.3026k
○ 8.5361k
Δ 82.8387k
Min -258.862...
Max 200.831...
IMA VERMILON
(A)
10.0k
-10.0k
× -0.0002k
○ -2.8049k
Δ -2.8047k
Min -8.4037k
Max 8.4061k
Total VMA
(V)
600.000k
-400.000k
× 166.9512k
○ 0.0140k
Δ -166.9372k
Min -401.421...
Max 519.007...
Phase Angle Difference
(Degree)
200
150
100
50
0
-50
-100
-150
-200
× -174.456
○ 0.022
Δ 174.478
Min -174.456
Max 179.214
t (S)
0.0
1.0
2.0
3.0
4.0
5.0
6.0
× 4.5
○ 1.5
Δ -3.0

a b

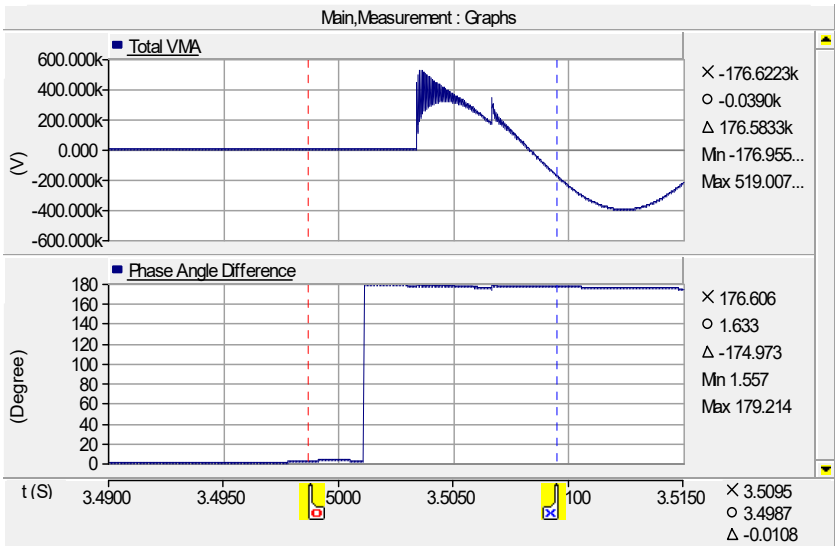
Main,Measurement : Graphs
Total VMA
(V)
600.000k
400.000k
200.000k
0.000
-200.000k
-400.000k
-600.000k
× -176.6223k
○ -0.0390k
Δ 176.5833k
Min -176.955...
Max 519.007...
Phase Angle Difference
(Degree)
180
160
140
120
100
80
60
40
20
0
× 176.606
○ 1.633
Δ -174.973
Min 1.557
Max 179.214
t (S)
3.4900
3.4950
5000
3.5050
100
3.5150
× 3.5095
○ 3.4987
Δ -0.0108

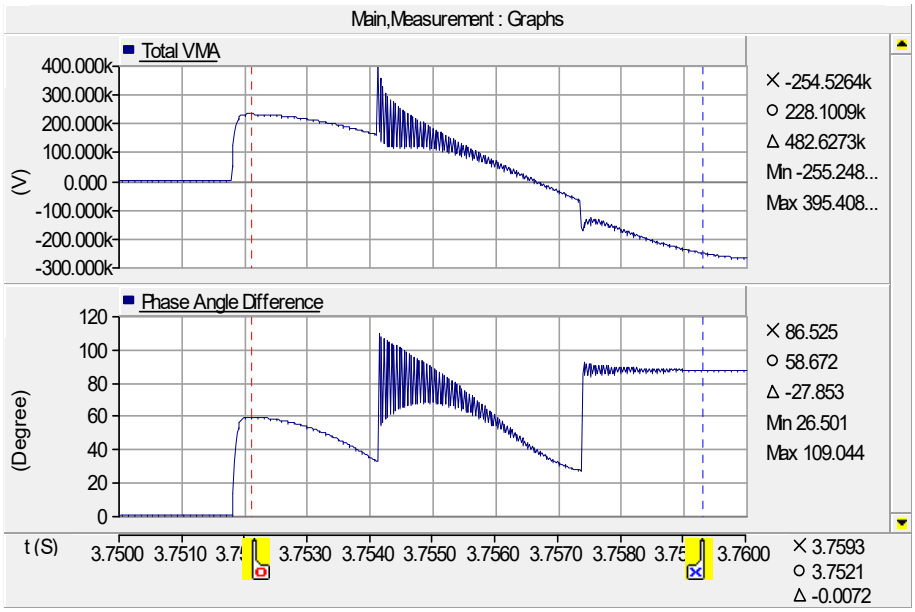

c d

Fig. 1.12: electrical quantities during switching disconnection in out of step condition, a) when phase angle difference is zero, b) when phase angle difference is 180°, c) close view of phase angle difference of 180°, d) close view of phase angle difference of 90°

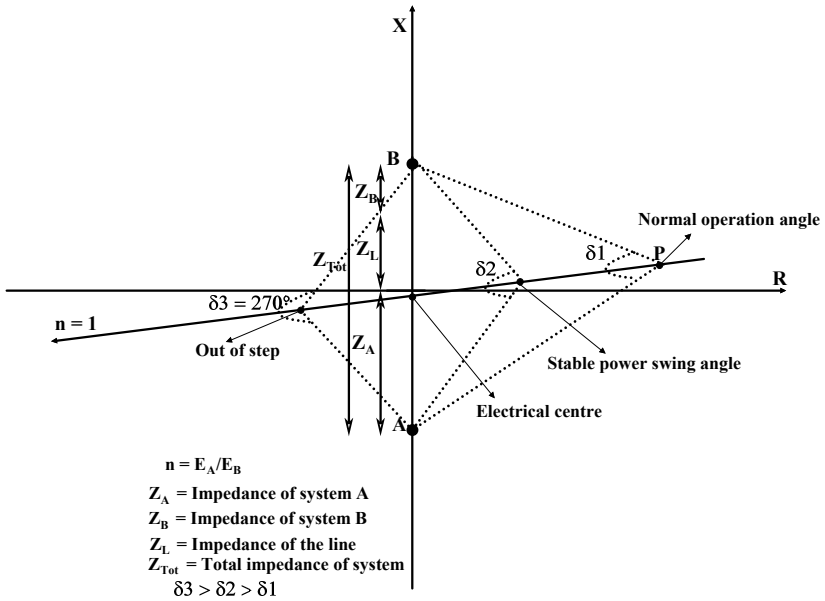

Fig. 1.13: Illustration of typical trip angle settable in protective relay during power swing

1-1-1- Sub Synchronous Resonance

Subsynchronous Resonance (SSR) is a phenomenon in which electrical energy is exchanged between generators and transmission systems below power frequency. SSR is caused by the interaction of a series-compensated transmission line with a rotary generation system, resulting in oscillation in the shaft and the occurrence of power swing in the grid. Additionally, SSR leads to an increase in the magnitudes of voltage and current, consequently causing ferroresonance in the network. In this section, the constituents and definitions of SSR are explained, along with the theoretical aspect of its occurrence in power networks.

1-1-3-1- Series compensation

Fig. 1.14 shows a simplified system diagram where a series-compensated transmission line interconnects two generating sources [14].

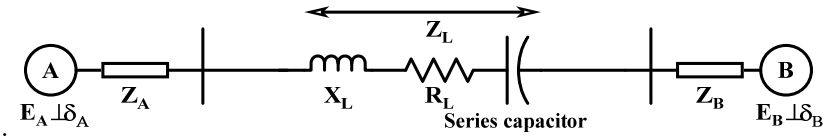

Fig. 1.14: A typical series compensated power system

Loadability of the AC transmission system is dependent on several factors such as line impedance, sending and receiving end voltages, and the phase angle between two ends as illustrated by (1.26).

$$P = \frac{V_S.V_R}{X_T}\sin\delta \tag{1.26}$$

Series compensation increases the loadability of power transmission by installing series capacitors, which decrease the total line impedance as follows:

$$X_T = X_L - X_C \tag{1.27}$$

$$X_T = (1 - S).X_L \tag{1.28}$$

S is the compensation degree, which varies between 0 and 100% as stated by:

$$S = \frac{X_C}{X_L} \times 100\% \tag{1.29}$$

Furthermore, series compensation improves power system transient stability, decreases reactive losses, and improves voltage regulation in the transmission system [14]. Theoretically, the degree of compensation can be determined as 100%; however, this may generate a large number of currents due to small disturbances or faults. The circuit contains series resonance at sub-fundamental frequencies. A high level of compensation can cause difficulties in protective relays and in the voltage profile during fault conditions. A practical limitation of compensation is 80%, but common values in current installations are in the order of 50%.

1-1-3-2- SSR phenomenon

Existing series capacitors in the power system cause emerging electrical resonance frequency in radial series-compensated lines. It is given by the following formula [15]:

$$f_{er} = \pm f_0\sqrt{\frac{X_C}{X_L}} \tag{1.30}$$

The circulation of the current under fer in the network flows in the armature winding of the generator and interacts with the generator shaft at frequencies of ω1-ω2 and ω1+ω2. The term of ω1-ω2 is the super synchronous frequency, where ω1-ω2 is the sub synchronous frequency. As shown in (1.31), the current includes both a fundamental component (network frequency) and a sinusoidal component that is dependent on elements of the network [4]:

$$i(t) = K[A\sin(\omega_1 t + \psi_1) + Be^{-\zeta\omega_2 t}\sin(\omega_2 t + \psi_2)] \tag{1.31}$$

Where A and B are constant
ζ is given by:

$$\zeta = \frac{R}{2}\sqrt{\frac{C}{L}} \tag{1.32}$$

ω_2 is calculated by:

$$\omega_2 = \omega_n\sqrt{1 - \zeta^2} \tag{1.33}$$

ω_n is calculated by:

$$\omega_n = \sqrt{\frac{1}{LC}} \tag{1.34}$$

Sub-synchronous current in the generator causes shaft torque in the turbine-generator, including the prime mover. Sub-synchronous torque can coincide with one of the natural frequencies of the rotary shaft, resulting in oscillation of the shaft at one of its natural frequencies. Sub-synchronous resonance can cause catastrophic damage to the turbine-generator shaft. Additionally, torsional oscillation in the shaft causes variation of load angle and can lead to the